Wetting and drying at a curved substrate: Long-ranged forces

M. C. Stewart* and R. Evans
H. H. Wills Physics Laboratory, University of Bristol, Bristol BS8 1TL, United Kingdom
(Received 14 September 2004; published 7 January 2005)

We examine the interfacial properties of a hard spherical cavity, radius R, immersed in a solvent in which the fluid-fluid interaction potential contains both a hard-sphere repulsive part and an attractive $-r^{-6}$ component. Near to liquid-gas coexistence where the chemical potential deviation $\delta\mu \equiv \mu - \mu_{co}(T) \to 0^+$ complete wetting by the gas (drying) occurs and a coarse-grained effective Hamiltonian approach shows that the wall/liquid surface tension has a term in $R^{-2/3}$, i.e., a leading-order power-law nonanalyticity in the curvature (R^{-1}) in the large cavity limit. For states sufficiently well removed from coexistence the surface tension can be expanded in integer powers of the curvature R^{-1}, provided $R > R_c$ with the length scale given by $R_c = 2\gamma_{gl}(\infty)/(\Delta\rho\delta\mu)$, where $\gamma_{gl}(\infty)$ is the planar liquid/gas surface tension and $\Delta\rho$ is the difference between the coexisting densities. However, even in these circumstances there are additional $R^{-2}\ln R$ contributions to the surface tension arising from the dispersion forces. An exact statistical mechanical sum rule is used to relate the density of the fluid at the point of contact with the cavity, $\rho(R^+, \mu)$, to the pressure of the reservoir and the surface tension. This predicts that $\rho(R^+, \mu)$ acquires a term in $R^{-5/3}$ in the regime $R < R_c$. Numerical results obtained by applying classical density functional theory to this model confirm all the predictions from the coarse-grained approach for both the surface tension and the contact density. We argue that our results for leading-order nonanalytic contributions are exact, i.e., they should remain valid in the presence of interface fluctuations, and we discuss briefly the repercussions for solvation phenomena and for other wetting situations.

DOI: 10.1103/PhysRevE.71.011602 PACS number(s): 68.08.Bc, 05.70.Np, 68.03.Cd

I. INTRODUCTION

Although the phenomenology of adsorption of simple fluids at planar substrates is, arguably, well understood, for curved substrates our understanding is relatively poorly developed. Much pioneering work on the relevant thermodynamics was carried out by Gibbs [1] and summaries of exact statistical mechanical results can be found in reviews by Henderson [2,3]. Understanding the role of curvature has taken on some new impetus because of recent advances in microfabrication techniques; these can be used to create geometrical or chemical structures, with various shapes and length scales, on solid substrates. How fluids behave in contact with such surfaces is important in microfluidics and is relevant for certain chemical and biological applications. In order to exploit fully the potential uses of structured substrates it is necessary to have a detailed understanding of a fluid's adsorption behavior and, in particular, its wetting properties [4]. Here we address a very basic question: How does the nature of adsorption change when a substrate that is planar acquires a nonzero curvature? We consider a particularly simple geometry, namely, that where the substrate is a hard spherical wall (or cavity) of radius R immersed in the fluid (solvent). Several recent studies [5] have focused on the case where the solvent is the hard-sphere fluid so there is no fluid-fluid phase separation and thus no complications of wetting or drying at the hard-wall–fluid interface. In these circumstances there are compelling arguments based on sum rules [6,7] and good numerical evidence from density functional theory (DFT) calculations [5,8] to support the conjecture that thermodynamic quantities such as the Gibbs adsorption and the surface excess free energy, as well as the fluid density in contact with the hard wall, can be expanded in integer powers of the curvature R^{-1}. If the solvent exhibits gas-liquid phase separation the situation becomes more complex and for large R and thermodynamic states sufficiently close to bulk coexistence, drying at the hard-wall–liquid interface leads to a regime where the surface thermodynamic quantities and the fluid contact density do not exhibit a power-series expansion in R^{-1}, rather recent studies predict striking nonanalytic behavior with terms depending on $\ln R$ [6,9]. However, these studies relate to a specific class of model where the fluid-fluid interaction potential is short ranged. This class includes potentials of finite support such as the truncated Lennard-Jones potential (as used in simulations) and the square-well model, but also includes exponentially decaying potentials. Since in real fluids dispersion forces are always present, it is important to enquire how results found for the class of short-ranged models are modified by the presence of long-ranged (power-law) interparticle potentials. It is well known from the phenomenology of complete wetting at planar substrates [10,11] that incorporating power-law forces leads to a very different type of nonanalyticity in surface thermodynamic functions. For example, in the complete wetting regime the Gibbs adsorption per unit area diverges as $-\ln \delta\mu$ for short-ranged forces but as $\delta\mu^{-1/3}$ for dispersion forces in three dimensions, in the limit where the chemical potential deviation from bulk coexistence $\delta\mu \equiv \mu - \mu_{co}(T)$ vanishes.

The specific model fluid we consider here has a pair potential consisting of a hard core of diameter σ plus an attractive tail, taken to be the attractive part of the full Lennard-Jones 12-6 potential—see Eq. (21) below. In the limit of a

*Electronic address: Maria.Thomas@bristol.ac.uk

planar substrate, $R=\infty$, such a fluid exhibits complete drying at the hard wall for all temperatures T for which there is bulk gas-liquid coexistence, i.e., a film of gas intrudes between the reservoir of the bulk liquid and the wall whose equilibrium thickness diverges, i.e., $l_{eq}\sim\delta\mu^{-1/3}$ as $\delta\mu\to 0^+$, for all $T<T_c$, the critical temperature. For a finite but large radius $R\gg\sigma$, we still expect to find a thick drying film but now its thickness will be limited by the curvature so that in the limit $\delta\mu=0^+$ l_{eq} remains finite. In the present case of dispersion forces, with the attractive fluid-fluid potential decaying as $-r^{-6}$, we find that $l_{eq}\sim R^{1/3}$, for $\delta\mu=0^+$, in agreement with earlier results based on an effective interfacial Hamiltonian approach [12–14]. By contrast, the corresponding result for short-ranged forces has $l_{eq}\sim\ln R$ [6,9,15]. Unlike previous studies of wetting on spheres and cylinders [12–17], where the main purpose was to investigate how nonzero curvature limits the equilibrium film thickness and modifies any wetting transitions that might occur at the planar substrate, we focus on the repercussions curvature has for the surface tension, i.e., the surface excess grand potential per unit area of the substrate, and on the behavior of the fluid density profile near the substrate. We find, in keeping with Ref. [6], that it is important to identify two separate regimes of interfacial behavior. For $R>R_c$, the surface tension and the density profile at the wall can be expanded in integer powers of R^{-1} whereas for $R<R_c$ these quantities acquire nonanalytic contributions, for example, the surface tension has a leading-order $R^{-2/3}$ correction to the planar value. The length scale $R_c\equiv 2\gamma_{gl}(\infty)/\delta\mu(\rho_l-\rho_g)$, where $\gamma_{gl}(\infty)$ is the planar gas-liquid surface tension and $(\rho_l-\rho_g)$ is the difference in coexisting densities, is the same as that which determines capillary condensation between two planar wetting walls or capillary evaporation between two planar hard walls [18].

Our paper is arranged as follows. In Sec. II we describe an effective interfacial Hamiltonian approach, based on a sharp-kink approximation for the fluid density profile around the hard-spherical cavity. By minimizing the excess grand potential as a function of the thickness of the drying film we determine the equilibrium thickness $l_{eq}(R,\mu)$ and the resulting wall-liquid surface tension. An exact statistical mechanical sum rule [2,3] is then used to obtain the fluid density $\rho(R^+,\mu)$ at the point of contact $r=R^+$ with the wall. The behavior of the surface tension and contact density in both regimes is identified. Section III describes a nonlocal DFT for our model fluid. The functional that we employ uses the Rosenfeld [19] fundamental measures theory to treat the hard-core repulsive part of the pair potential while treating the long-ranged attractive tail $\phi_{att}(r)$ in a simple mean-field fashion: for a uniform fluid the pair direct correlation function resulting from our functional is $c(r)=c_{hs}(r)-\beta\phi_{att}(r)$, where $\beta=(k_BT)^{-1}$ and $c_{hs}(r)$ is the hard-sphere direct correlation function obtained from Percus-Yevick theory. The density profiles and thermodynamic functions which result from minimizing this functional are known to satisfy both the Gibbs adsorption theorem and the sum rule for the contact density [9]. This consistency is crucially important when seeking subtle effects, especially contributions to thermodynamic quantities that are nonanalytic in some parameter. In Sec. IV we present the results of our numerical DFT calculations, comparing with the predictions from the mesoscopic treatment of Sec. II. We find that all these predictions are borne out by the numerical results for both regimes, i.e., for $R>R_c$ and $R<R_c$, confirming the validity of the coarse-grained effective Hamiltonian approach. Section V considers the adsorption of the model fluid *inside* the hard spherical cavity, i.e., the situation of negative curvature, where capillary evaporation is relevant. We conclude in Sec. VI with a discussion of our results and their possible significance for other interfacial phenomena. The Appendix describes the sharp-kink calculation of the surface tension for fluid-fluid and wall-fluid interfaces and of the binding potential that enters the effective interfacial Hamiltonian used in Sec. II. The sharp-kink treatment predicts that for both fluid-fluid and wall-fluid interfaces the surface tension contains a leading-order correction to the planar result which is proportional to $R^{-2}\ln R$ when dispersion forces are present [12,20]. The existence of this contribution was confirmed in our DFT calculations for a hard-wall–*gas* interface where there are no complications of drying. Note, however, that within DFT the leading-order correction is $O(R^{-1})$. For the hard-wall–*liquid* interface drying leads to stronger, $R^{-2/3}$, leading-order corrections to the surface tension.

Although our calculations pertain directly to the situation of complete drying at a hard spherical wall, it should be recognized [6,9] that our results concerning nonanalytic features in surface thermodynamic functions and crossover from analytic to nonanalytic behavior are equally relevant to several other (less esoteric) physical problems. These include (i) wetting films of liquid adsorbed from the gas close to saturation on the surfaces of curved substrates, and (ii) wetting of spherical colloidal particles immersed in a phase separating (binary) solvent. If the colloid preferentially adsorbs one component of the mixture a wetting film of the phase rich in that component can develop on the colloids and this leads subsequently to a variety of interesting phenomena, including attractive effective interactions, bridge formation, and possible coagulation of the colloidal particles [12,21,22]. It is also important to consider potential implications of our results for understanding the physics and chemistry of solvation. Chandler and co-workers [23] have argued that a proper understanding of hydrophobic effects, at varying length scales, should incorporate drying phenomena. In particular they point to the importance of the length scale R_c, which is ~ 1 μm for water at room temperature and pressure [6]. We discuss briefly the repercussions of our work for determining solvation free energies, i.e., the work required to insert a hard-spherical cavity into a solvent, as a function of cavity radius and solvent chemical potential, leaving a more detailed treatment to a later paper.

II. THE EFFECTIVE INTERFACIAL POTENTIAL

We begin with a coarse-grained effective Hamiltonian approach as used in Ref. [9]; for general reviews see Refs. [10,11]. In this, sharp-kink, approximation the density of the fluid at a hard spherical wall (radius R) is taken to be

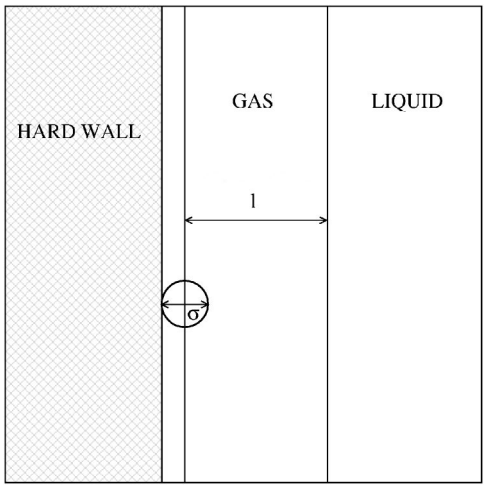

FIG. 1. Geometry for a hard-sphere fluid in contact with a planar wall, showing a fluid particle of diameter σ at the contact surface for the density profile ($h=0$). In the sharp-kink approximation for drying there is a film of fluid with the gasdensity ρ_g^+ between $h=0$ and $h=l$. For $h>l$ the density is that of the bulk liquid ρ.

$$\rho(r) = \begin{cases} 0, & r < R, \\ \rho_g^+, & R < r < R + l, \\ \rho, & r > R + l, \end{cases} \tag{1}$$

where ρ is the density of the liquid reservoir at chemical potential μ and ρ_g^+ is the density of the (metastable) gas at the same value of μ. This is illustrated in Figs. 1 and 2; Fig. 1 shows the planar system ($R=\infty$). The excess (over bulk) grand potential is then written as a function of the drying film thickness l,

$$\Omega^{ex} \equiv \Omega + pV_{acc} = \gamma_{wg}(R,\mu)A_{wg} + \gamma_{gl}(R+l)A_{gl} + \omega(l;R)A_{wg} + (p - p_g^+)V_g \tag{2}$$

where the accessible volume $V_{acc}=V_{total}-4\pi R^3/3$, p is the pressure of the liquid reservoir, and p_g^+ is the pressure of the (metastable) gas. For small values of $\delta\mu \equiv \mu - \mu_{co}(T)$, the deviation from bulk coexistence, the pressure difference

$$p - p_g^+ = (\rho_l - \rho_g)\delta\mu \tag{3}$$

where ρ_l and ρ_g are the bulk coexisting densities at temperature T. $V_g=4\pi[(R+l)^3-R^3]/3$ is the volume of the gas drying film. The first two terms in Eq. (2) are surface contributions: $\gamma_{wg}(R,\mu)$ and $\gamma_{gl}(R+l)$ are the surface tensions of the wall/gas and gas/liquid interfaces and A_{wg} and A_{gl} are the corresponding areas. The interaction between the two interfaces is given by the third term and the binding potential, $\omega(l;R)$, is derived using the sharp-kink approximation in the Appendix. For the particular case of drying at a hard-spherical surface one finds [see Eq. (A14)]

$$\omega(l;R) = \omega(l;\infty)\left[1 + \frac{l}{R} + O\left(\frac{l^2}{R^2}\ln\left(\frac{l}{2R}\right)\right)\right] \tag{4}$$

with the planar limit of the binding potential given by

$$\omega(l;\infty) = \frac{b}{l^2} + O\left(\frac{1}{l^8}\right) \tag{5}$$

where the coefficient of the familiar l^{-2} term is

$$b = \rho_g(\rho_l - \rho_g)\pi\epsilon\sigma^6/3. \tag{6}$$

b is the energy parameter (or the Hamaker constant) appropriate for hard-wall drying in a fluid in which the attractive part of the fluid-fluid pair potential is given by a Lennard-Jones (LJ) form—see Eq. (21) below. ϵ is the LJ well depth and σ is the diameter.

In the planar limit ($R=\infty$) minimization of Eq. (2), with Eq. (5), yields complete drying for *all* temperatures $T<T_c$, the bulk critical temperature, since the parameter b is always positive. That is, in the limit $\delta\mu \to 0^+$, the equilibrium film thickness $l_{eq}\to\infty$ and $\Omega^{ex}/A_{wg} \to \gamma_{wg}(\infty,\mu_{co}) + \gamma_{lg}(\infty)$.

For the spherical case we assume $l_{eq} \ll R$ and expand in powers of l/R in Eq. (2):

$$\frac{\Omega^{ex}}{A_{wg}} = \gamma_{wg}(R,\mu) + \gamma_{gl}(R)\left(1 + \frac{2l}{R}\right) + \frac{b}{l^2} + (\rho_l - \rho_g)\delta\mu l \tag{7}$$

and we have ignored the difference between $\gamma_{gl}(R)$ and $\gamma_{gl}(R+l)$. Higher order terms are not displayed.

Minimizing Eq. (7) with respect to l gives the equilibrium drying film thickness

$$l_{eq} = \left(\frac{2b}{(\rho_l - \rho_g)\delta\mu + 2\gamma_{gl}(\infty)/R}\right)^{1/3} \tag{8}$$

where, consistent with the leading-order analysis, the planar value is used for the gas-liquid surface tension $\gamma_{gl}(R)$. In the limit $\delta\mu \to 0$, Eq. (8) predicts that the drying film thickens as $R^{1/3}$ [12–14]. The nonzero Laplace pressure arising from the curved gas-liquid interface prevents the film thickness from diverging. The key observation from Eqs. (7) and (8) is that within this coarse-grained effective Hamiltonian approach the undersaturation pressure $(\rho_l - \rho_g)\delta\mu$ plays the same role as the Laplace pressure $2\gamma_{gl}(\infty)/R$. More specifically, the equilibrium thickness of the drying film at bulk coexistence

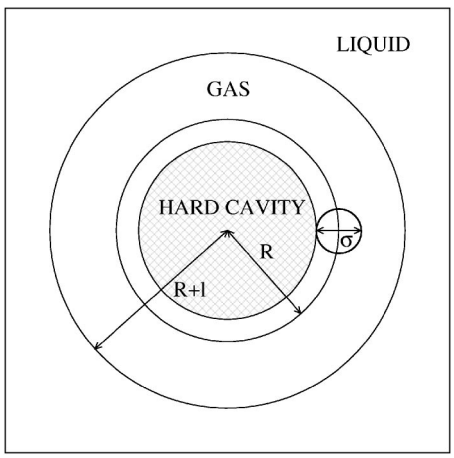

FIG. 2. The equivalent system in spherical geometry showing a fluid particle at the contact radius for the density profile ($r=R$). In the sharp-kink approximation there is a film of fluid with the gas density ρ_g^+ between $r=R$ and $r=R+l$. For $r>R+l$ the density is that of the bulk liquid ρ.

on the spherical substrate is equal to that for the same fluid at a planar substrate when the reservoir is at a chemical potential deviation $\delta\mu = 2\gamma_{lg}/R(\rho_l - \rho_g)$. This equivalence between the two pressures has been recognized by several authors, e.g., Refs. [12,15–17]. Less well recognized are the implications for the excess grand potential and its derivatives with respect to thermodynamic fields [6,9] and it is these implications that we investigate here for the case of dispersion forces, i.e., for a fluid-fluid pair potential decaying as $-r^6$.

Substituting Eq. (8) into Eq. (7) gives the equilibrium wall-liquid surface tension, shown to leading order:

$$\gamma_{wl}(R,\mu) \equiv \Omega_{eq}^{ex}/4\pi R^2 = \gamma_{wg}(R,\mu) + \gamma_{gl}(R) + \tfrac{3}{2}(2b)^{1/3}\tilde{p}^{2/3} \tag{9}$$

where

$$\tilde{p} \equiv (\rho_l - \rho_g)\,\delta\mu + \frac{2\gamma_{gl}(\infty)}{R}. \tag{10}$$

For a planar hard wall ($R=\infty$) the surface tension in the sharp-kink approximation reduces to

$$\gamma_{wl}(\infty,\mu) = \gamma_{wg}(\infty,\mu) + \gamma_{gl}(\infty) + \tfrac{3}{2}(2b)^{1/3}[(\rho_l - \rho_g)\,\delta\mu]^{2/3} \tag{11}$$

which implies that the critical exponent characterizing the free energy for complete drying is $\alpha_s^{co} = 4/3$ [10,11]. If one attempts a microscopic treatment, beyond the sharp kink, then a term linear in $\delta\mu$ should arise, in addition to possible higher order nonanalytic terms.

The curvature dependence of the (nondrying) wall/gas and gas/liquid surface tensions is the subject of much literature, e.g., [2,12,20,24–27]. In the Appendix we use the sharp-kink approximation to calculate the surface tension for both interfaces. For dispersion forces there are [12,20] $R^{-2}\ln R$ corrections to the planar limiting values—see Eq. (A12) but note that within the sharp-kink approximation there is no term in R^{-1}, i.e., the Tolman [24] length is identically zero. However, beyond the sharp-kink approximation it is likely that the leading-order corrections are proportional to R^{-1}, so we assume

$$\gamma_{wg}(R,\mu) = \gamma_{wg}(\infty,\mu)\left[1 - \frac{2\delta_T^{wg}}{R} + O\left(\frac{\ln(R)}{R^2}\right)\right], \tag{12}$$

$$\gamma_{gl}(R) = \gamma_{gl}(\infty)\left[1 - \frac{2\delta_T^{gl}}{R} + O\left(\frac{\ln(R)}{R^2}\right)\right], \tag{13}$$

where δ_T^{wg} and δ_T^{gl} are the Tolman lengths for the wall/gas and gas/liquid interfaces, respectively. [Explicit results for the planar tensions derived from the sharp-kink approximation are given in the Appendix—see Eqs. (A7) and (A8).] Setting $\delta\mu = 0$ in Eq. (9) and employing Eqs. (12) and (13) we find that the wall/liquid surface tension for the hard-spherical substrate with liquid at bulk coexistence reduces to

$$\gamma_{wl}(R,\mu_{co}^{+}) = \gamma_{wg}(\infty,\mu_{co}) + \gamma_{gl}(\infty) + 3\left(\frac{\gamma_{gl}(\infty)^2 b}{R^2}\right)^{1/3} + \Sigma\frac{\delta_T}{R} + O(R^{-4/3}), \tag{14}$$

where δ_T is some microscopic length and Σ has the dimensions of surface tension. This term, in R^{-1}, which arises from contributions beyond the sharp kink, combines contributions from the surface tensions of the wall/gas and gas/liquid interfaces and from the binding potential. Note that the leading-order curvature correction varies as $R^{-2/3}$, implying that the first derivative of γ_{wl} with respect to the curvature R^{-1} would diverge in the limit $R^{-1}\to 0$.

This striking nonanalytic behavior of a thermodynamic quantity is the analog for a power-law fluid-fluid potential of the result found in Ref. [9] for drying with short-ranged potentials. There the corresponding nonanalytic contribution to the surface tension varies as $R^{-1}\ln(aR)$, where the constant a is not known. In the present case the parameter b is determined, once the pair potential is specified and the coexisting densities are determined—see Eq. (6). Note that in Eq. (14) we have not included the higher-order $R^{-2}\ln R$ contributions.

We can use the results derived above to calculate the density of the fluid at the point of contact $\rho(R^+,\mu)$. There is an exact statistical mechanical sum rule [2] relating the contact density at a hard wall to the wall/fluid surface tension γ_{wf} and the bulk pressure p:

$$k_B T\rho(R^+,\mu) = p + \frac{2\gamma_{wf}}{R} + \left(\frac{\partial\gamma_{wf}}{\partial R}\right)_{T,\mu}. \tag{15}$$

Note that in the planar limit, $R^{-1}\to 0$, the contact density reduces to the well-known result $\rho(0^+,\mu) = p/k_B T$. If we set $\delta\mu = 0^+$ we can employ Eq. (14) and we find for the contact density of the liquid at coexistence

$$k_B T\rho(R^+,\mu_{co}^{+}) = p + \frac{2\gamma_{wg}(\infty,\mu_{co})}{R} + \frac{2\gamma_{gl}(\infty)}{R} + 4\left(\frac{\gamma_{gl}(\infty)^2 b}{R^5}\right)^{1/3} + O(R^{-2}). \tag{16}$$

This result is interesting for two reasons: (i) it states that the contact density depends on the surface tension of the gas/liquid interface, which can be very far from the wall ($l_{eq} \sim R^{1/3}$) when R is very large and (ii) the contact density acquires a term $\propto R^{-5/3}$ which is nonanalytic in the curvature (R^{-1}). The corresponding term for a short-ranged potential varies as $R^{-2}\ln(aR)$ [9].

Of course one need not proceed directly to the limit $\delta\mu = 0$. As pointed out in Ref. [12] and discussed in detail for short-ranged forces in Ref. [6] one should distinguish between two regimes of interfacial behavior as defined by the length scale

$$R_c \equiv \frac{2\gamma_{gl}(\infty)}{(\rho_l - \rho_g)\,\delta\mu}. \tag{17}$$

For the regime $R \ll R_c$ for which $\delta\mu$ must be kept very small (recall that $R \gg \sigma$ for the coarse-grained approach to be applicable) we recover, at leading order, the results (14) and (16); the leading-order corrections to these results are linear in $\delta\mu$. On the other hand, for $R \gg R_c$, which corresponds to

approaching the planar limit at nonzero $\delta\mu$, we expand $\tilde{p}$ in powers of R_c/R in Eq. (9) and find

$$\gamma_{wl}(R,\mu) = \gamma_{wl}(\infty,\mu) + \frac{2\gamma_{gl}(\infty)}{R}\left(\frac{2b}{(\rho_l-\rho_g)\delta\mu}\right)^{1/3} + \frac{\Sigma\delta_T}{R} + O(R^{-2}\ln R) + O\left(\frac{R_c}{R}\right)^2 \tag{18}$$

where the planar surface tension $\gamma_{wl}(\infty,\mu)$ is given by Eq. (11). In this regime one has a power series in the curvature R^{-1}, as for the case of short-ranged potentials [6], but there are additional $R^{-2}\ln R$ terms arising from dispersion forces, Eqs. (12) and (13), which we now include explicitly. Since $\Sigma\delta_T$ should depend very weakly on $\delta\mu$, the coefficient of the R^{-1} contribution in Eq. (18) should increase as $\delta\mu^{-1/3}$ when $\delta\mu$ is reduced at fixed large R, provided one remains in the regime $R_c \ll R$; we cannot allow $\delta\mu$ to vanish.

Similarly one can calculate the contact density in the same regime, $R \gg R_c$, and obtain

$$k_BT\rho(R^+,\mu) = p + \frac{2\gamma_{wl}(\infty,\mu)}{R} + O(R^{-2}). \tag{19}$$

Thus from the coefficient of the R^{-1} term in the contact density one can obtain the planar surface tension at nonzero $\delta\mu$. This contains the nonanalytic $\delta\mu^{2/3}$ term [see Eq. (11)] associated with complete drying. The remaining contributions in Eq. (19) constitute a power series in the curvature R^{-1}; cf. [6]. Note that there is no $R^{-3}\ln R$ contribution.

The results presented above pertain to a coarse-grained effective Hamiltonian description of the drying film. One might expect that the *form* of the leading-order results is maintained in a fully microscopic treatment in which the surface tensions are not those obtained from the sharp-kink approximation; rather they are those obtained from a proper microscopic theory. In Refs. [6,9] this assertion was tested for a square-well fluid. Here we examine the predictions of the coarse-grained theory for a model fluid with a hard core plus a power-law attractive potential using the same DFT as used in Refs. [6,9]. In this case the predictions involve power-law nonanalyticities rather than logarithms and, significantly, we know the relevant *amplitudes*, since these depend on the energy parameter b, whose value is determined.

III. DENSITY FUNCTIONAL THEORY

In density functional theory the free energy of an inhomogeneous fluid is expressed as a functional of the average one-body density $\rho(\mathbf{r})$. DFT methods are widely used to investigate equilibrium structure and thermodynamic functions such as surface tensions. For a review of DFT see Ref. [28]. The free-energy functional is not known exactly. In the approximation that we employ the attractive part of the intrinsic Helmholtz free energy functional is treated as a type of perturbation about a hard-sphere reference fluid:

$$\mathcal{F}[\rho] = \mathcal{F}_{id}[\rho] + \mathcal{F}_{hs}[\rho] + \frac{1}{2}\int d\mathbf{r}_1 \int d\mathbf{r}_2 \rho(\mathbf{r}_1)\rho(\mathbf{r}_2)\phi_{att}(r_{12}) \tag{20}$$

where $r_{12}=|\mathbf{r}_1-\mathbf{r}_2|$. The ideal gas term is simply

$$\beta\mathcal{F}_{id}[\rho] = \int d\mathbf{r}\, \rho(\mathbf{r})[\ln \Lambda^3\rho(\mathbf{r}) - 1]$$

where $\beta = 1/(k_BT)$ and Λ is the thermal de Broglie wavelength.

Our model fluid has a hard-sphere repulsive core and for the attractive interaction potential between fluid particles we use the attractive part of the Lennard-Jones potential:

$$\phi_{att}(r) = \begin{cases} 4\epsilon\left[\left(\frac{\sigma}{r}\right)^{12} - \left(\frac{\sigma}{r}\right)^{6}\right], & r > r_{min}, \\ -\epsilon, & r < r_{min}, \end{cases} \tag{21}$$

where $r_{min} = 2^{1/6}\sigma$.

The hard-sphere part of the excess free-energy functional $\mathcal{F}_{hs}[\rho]$ is treated by means of Rosenfeld's fundamental measures theory [19]. His functional for a single-component hard-sphere fluid is

$$\beta\mathcal{F}_{hs}[\rho] = \int d\mathbf{r}\, \Phi(n_\alpha), \tag{22}$$

where the reduced free-energy density is taken to be

$$\Phi(n_\alpha) = -n_0\ln(1-n_3) + \frac{n_1n_2 - \mathbf{n}_1\cdot\mathbf{n}_2}{1-n_3} + \frac{n_2^3 - 3n_2\mathbf{n}_2\cdot\mathbf{n}_2}{24\pi(1-n_3)^2}.$$

The weighted densities n_α are calculated from

$$n_\alpha(\mathbf{r}_1) = \int d\mathbf{r}_2 \rho(\mathbf{r}_2) w_\alpha(\mathbf{r}_1-\mathbf{r}_2), \tag{23}$$

where the four scalar weight functions for hard spheres of diameter σ are

$$w_3(\mathbf{r}) = \Theta(\sigma/2 - r), \quad w_2(\mathbf{r}) = \delta(\sigma/2 - r),$$

$$w_1(\mathbf{r}) = \frac{w_2(\mathbf{r})}{2\pi\sigma}, \quad w_0(\mathbf{r}) = \frac{w_2(\mathbf{r})}{\pi\sigma^2}$$

and the two vector weight functions are given by

$$\mathbf{w}_2(\mathbf{r}) = \frac{\mathbf{r}}{r}\delta(\sigma/2 - r), \quad \mathbf{w}_1(\mathbf{r}) = \frac{\mathbf{w}_2(\mathbf{r})}{2\pi\sigma}.$$

For the homogeneous hard-sphere fluid the free-energy density reduces to the Percus-Yevick compressibility result and the pair direct correlation function obtained by taking two functional derivatives of $\mathcal{F}_{hs}[\rho]$ is identical to that from Percus-Yevick theory [19]. This weighted-density approximation incorporates short-range correlations so that oscillatory density profiles can result. Moreover it also describes correctly the density at the hard wall so that the sum rule [Eq. (15)] and the Gibbs adsorption theorem are satisfied. This was confirmed earlier in numerical studies for hard spheres adsorbed at hard curved cavities [5] and checked carefully in the present study for the functional (20). In our calculations we take the hard-sphere diameter σ to be equal to the diameter entering the Lennard-Jones potential (21).

The equilibrium density profile is found by minimizing the grand potential functional:

$$\Omega_v[\rho] = \mathcal{F}[\rho] - \int d\mathbf{r}[\mu - V(\mathbf{r})]\rho(\mathbf{r}) \tag{24}$$

where μ is the chemical potential and $V(\mathbf{r})$ is the external hard-wall potential,

$$V(\mathbf{r}) = \begin{cases} +\infty, & r \leqslant R, \\ 0 & \text{otherwise}. \end{cases} \tag{25}$$

Applying the variational principle with Eq. (20) gives the Euler-Lagrange equation

$$\mu = V(\mathbf{r}_1) + \mu_{id}(\rho(\mathbf{r}_1)) + \frac{\delta \mathcal{F}_{hs}[\rho]}{\delta \rho(\mathbf{r}_1)} + \int d\mathbf{r}_2 \rho(\mathbf{r}_2)\phi_{att}(\mathbf{r}_1 - \mathbf{r}_2) \tag{26}$$

where μ_{id} is the ideal gas chemical potential. The third term in Eq. (26) is evaluated by substituting Eq. (23) into Eq. (22) and taking the derivative to obtain

$$\beta \frac{\delta \mathcal{F}_{hs}[\rho]}{\delta \rho(\mathbf{r}_1)} = \int d\mathbf{r}_2 \sum_\alpha \frac{\partial \Phi}{\partial n_\alpha} w_\alpha(\mathbf{r}_1 - \mathbf{r}_2). \tag{27}$$

Note that the final term in Eq. (26), which constitutes a simple mean-field-like contribution to the intrinsic chemical potential, is long ranged for power-law potentials such as Lennard-Jones. Equation (26) was solved numerically to find the equilibrium density profile. From this the corresponding equilibrium excess grand potential Ω_{eq}^{ex} was calculated. Note that in our calculations the dividing surface is located at $r = R^+$, the radius where the density profile first becomes nonzero. The physical radius of the hard wall is $R - \sigma/2$—see Figs. 1 and 2. The liquid-gas coexistence curve is determined from the bulk free energy obtained by setting $\rho(\mathbf{r})$ to be constant in Eq. (20). The critical temperature is given by $k_B T_c/\epsilon = 1.415\,39$.

IV. NUMERICAL RESULTS

A. Wall/gas surface tension

Initially the curvature dependence of the wall/gas surface tension was investigated. For this situation no drying film is present. DFT results for a hard-sphere fluid at a hard-spherical wall [5,8] suggest that the leading-order correction to the planar surface tension is linear in the curvature. They show no evidence for the existence of logarithmic terms. Rather the surface tension and the contact density are accurately represented by power-series expansions in R^{-1}. When long-ranged dispersion forces between the fluid molecules are introduced then a nonanalytic $R^{-2}\ln R$ term is predicted by the sharp-kink approximation—see Eq. (12).

In Fig. 3 we display the results for the surface tension as a function of curvature for a state at bulk coexistence, $\mu = \mu_{co}^-(T)$, with $T = 0.7T_c$ for which the coexisting densities are $\rho_g\sigma^3 = 0.018\,026$ and $\rho_l\sigma^3 = 0.667\,379$. A least squares fit to the data gives a positive coefficient for the R^{-1} term which corresponds to a small negative Tolman length. This term has contributions from both the short-ranged repulsive hard-sphere potential and from the attractive Lennard-Jones potential. The sharp-kink approximation for the surface tension does not have an R^{-1} term but if a more realistic profile is assumed then such contributions do arise from the dispersion forces.

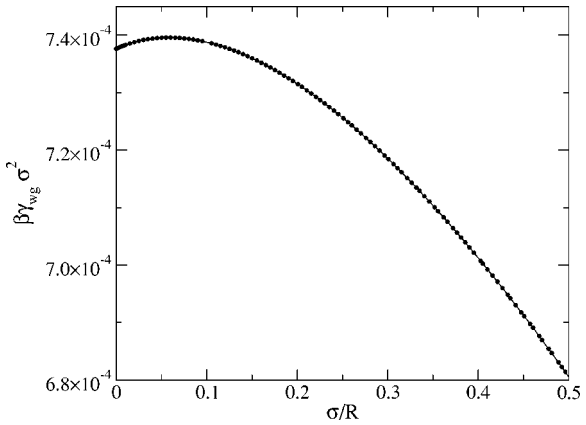

FIG. 3. Surface tension of the gas at a hard-spherical wall of radius $R - \sigma/2$, at $T = 0.7T_c$ and $\mu = \mu_{co}^-$, (●). The line is a fit to the equation $\beta\sigma^2\gamma_{wg}(R) = a_0 + a_1\sigma/R + a_{2\,\ln}(\sigma/R)^2\ln(2R/r_{min}) + a_2(\sigma/R)^2$. The resulting coefficients are $a_0 = 7.3765 \times 10^{-4}$, which is close to the independently determined planar surface tension $\beta\sigma^2\gamma_{wg}(\infty) = 7.3763 \times 10^{-4}$, $a_1 = 7.7 \times 10^{-5}$ giving a negative Tolman length $\delta_T^{wg}/\sigma = -a_1/(2a_0) = -0.05$, $a_{2\,\ln} = -1.70 \times 10^{-4}$ (sharp-kink prediction $= -1.72 \times 10^{-4}$), and $a_2 = -1.7 \times 10^{-4}$ (sharp-kink prediction $= -1.4 \times 10^{-4}$).

The coefficient of the $R^{-2}\ln R$ term extracted from the fit can be compared with the value predicted by the sharp-kink approximation [Eq. (A11)]. The agreement is about 1 part in 100. Numerical results at other state points show similar consistency. This is convincing numerical evidence for the presence of the $R^{-2}\ln R$ nonanalytic contribution to the surface tension. The close agreement between the numerical (DFT) and sharp-kink values for this coefficient is perhaps surprising since the DFT density profiles are not sharp-kink-like, as the nonzero Tolman length clearly illustrates. However, it is unlikely that deviations from the sharp-kink behavior in the density profiles (which give rise to the R^{-1} term and alter the coefficient of R^{-2}) could lead to any additional $R^{-2}\ln R$ terms in the surface tension. Indeed our analysis suggests that the coefficient of $R^{-2}\ln R$ depends only on the bulk densities of the two phases so that the sharp-kink value remains correct even when the microscopic profile is not sharp-kink-like.

The sharp-kink approximation also yields a value for the coefficient of the R^{-2} contribution. This is similar to the value we obtain from fitting to our DFT data (see caption to Fig. 3) but is not identical because of corrections from the hard-sphere part of the potential and from the (non-sharp-kink) shape of the profile.

B. Wall/liquid (drying) density profiles

Figure 4 shows density profiles for the liquid at bulk coexistence, $\mu_{co}^+(T)$, at the same temperature $T = 0.7T_c$, in contact with large hard spheres of various radii. Provided R is sufficiently large these profiles are nearly identical to those at

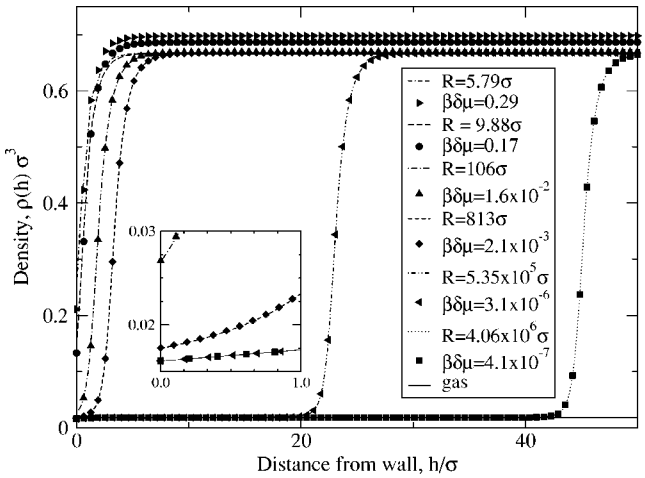

FIG. 4. Density profiles of the liquid adsorbed at hard walls for $T=0.7T_c$. The broken curves refer to the liquid at bulk coexistence, $\mu_{co}^{+}(T)$, at spherical walls of various radii $R-\sigma/2$. The symbols refer to the liquid near a planar wall at chemical potential deviation $\delta\mu \equiv \mu-\mu_{co}(T)=2\gamma_{gl}(\infty)/[R(\rho_l-\rho_g)]$. For each radius, except the two smallest ones, the two profiles are indistinguishable. The solid line refers to the gas at $\mu_{co}^{-}(T)$ at a planar wall. The inset shows the region very close to the wall.

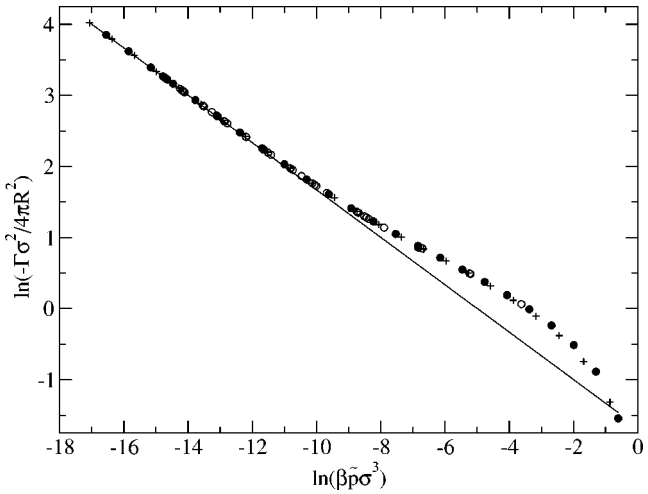

FIG. 5. Log-log plot of adsorption per unit area versus $\beta\tilde{p}\sigma^3 \equiv[(\rho_l-\rho_g)\delta\mu+2\gamma_{lg}(\infty)/R]\beta\sigma^3$ at $T=0.7T_c$. The DFT data correspond to a liquid adsorbed at spherical walls of different radii, $R-\sigma/2$, both at coexistence (●) and off coexistence at various $\delta\mu \equiv \mu-\mu_{co}(T)$ (○). There are also data for a liquid off coexistence, adsorbed at a planar hard wall (+). The straight line with slope $-1/3$ is the prediction of Eq. (8).

a planar hard wall with $\delta\mu=2\gamma_{gl}(\infty)/[R(\rho_l-\rho_g)]$. This equivalence of microscopic density profiles was also observed for systems with short-ranged potentials [9]. It holds down to quite a small radius ($R\approx 10\sigma$), where there is no thick drying film and where the relevant bulk densities are clearly different. This is a surprising result, first because the equivalence between bulk field (undersaturation pressure) for a planar wall and curvature (Laplace pressure) predicted by Eq. (8) might be expected to apply only to the film thickness l_{eq}, not necessarily to the whole microscopic profile. Second, one observes in Fig. 4 that the shapes of the profiles for $R<100\sigma$ are far from the sharp-kink profile assumed in the derivation of Eq. (8).

The inset demonstrates that for $R\geqslant 5\times 10^5\sigma$, when there is a very thick drying film present, the density close to the wall approaches that of the bulk coexisting gas, $\mu=\mu_{co}^{-}(T)$, at a planar wall. Therefore we expect that the total wall/liquid surface tension can indeed be written as the sum of the separate wall/gas and gas/liquid tensions plus a term for the interaction between the two interfaces. For smaller values of R one sees that the density near contact with the wall is greater than that for the gas at coexistence but the equivalence between the profiles for the two wall/liquid interfaces remains valid.

C. Adsorption at the wall/liquid interface

Within the effective Hamiltonian approach the drying film thickness l is the natural variable. The corresponding thermodynamic quantity is the Gibbs adsorption

$$\Gamma(R,\mu)=4\pi\int_R^\infty r^2[\rho(r)-\rho]dr, \tag{28}$$

where ρ is the reservoir density. Within DFT the adsorption was found by numerically integrating the density profile. It can also be obtained from the relation $\Gamma=-\partial\Omega_{eq}^{ex}(R,\mu)/\partial\mu$. An equilibrium film thickness can then be defined via

$$l_{eq}\equiv-\frac{\Gamma(R)}{4\pi R^2(\rho_l-\rho_g)}. \tag{29}$$

Figure 5 shows a log-log plot of adsorption per unit area versus the (dimensionless) pressure $\beta\tilde{p}\sigma^3\equiv[(\rho_l-\rho_g)\delta\mu+2\gamma_{lg}(\infty)/R]\beta\sigma^3$ [see Eq. (10)]. The data include adsorption at a planar substrate for a liquid off coexistence and adsorption at spherical substrates on and off coexistence. The adsorption predicted by substituting Eq. (8) into Eq. (29) is shown as a straight line on the plot. In the region where the magnitude of the adsorption and therefore the drying film thickness is large ($l_{eq}>12\sigma$) this line gives a good fit to the numerical results. For thinner drying films the sharp-kink approximation appears to break down, although the equivalence between the pressures, $2\gamma_{lg}(\infty)/R$ and $(\rho_l-\rho_g)\delta\mu$ holds even when the sphere radius is small and there is no thick drying film, i.e., the data for the planar and curved walls still collapse onto a single curve.

D. Wall/liquid surface tension

In Fig. 6 we plot the difference between the wall/liquid and wall/gas surface tensions (at $\mu_{co}^{\pm}$) for $T=0.7T_c$ versus σ/R for very large values of R/σ. According to Eq. (14) we expect the leading-order correction to the planar gas-liquid tension to be $3[\gamma_{gl}(\infty)^2 b]^{1/3}\ R^{-2/3}$. A least squares fit to the numerical DFT data permits a comparison with the predicted coefficient of the $R^{-2/3}$ term. The latter was calculated using the theoretical (sharp-kink) value for b [Eq. (6)] which gives $\beta b=0.012\,372$ for this temperature and the numerical result for the planar liquid/gas surface tension: $\beta\sigma^2\gamma_{gl}(\infty,\mu)=0.545\,196$. The agreement is better than 0.2%.

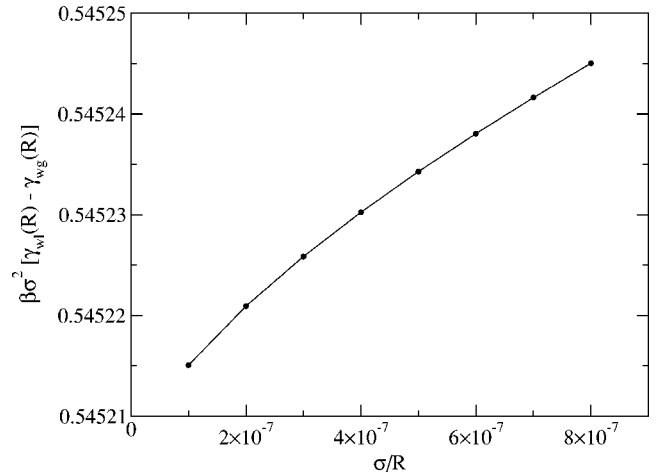

FIG. 6. The difference between the surface tensions in the liquid, at $\mu_{co}^{+}(T)$, and gas, $\mu_{co}^{-}(T)$, phases, adsorbed at hard-spherical walls of radius $R-\sigma/2$, versus curvature for $T=0.7T_c$ (●). The line shows a fit to the DFT data assuming $R^{-2/3}$ dependence (see text).

In order to test the validity of the expansion of the surface tension in powers of R^{-1} for $R>R_c$ [Eq. (18)], the surface tension is plotted as a function of curvature at two different fixed chemical potentials near coexistence. The results, for large radius, are shown in Figs. 7 and 8. The intercepts of the linear fits give excellent agreement with the independently calculated, within DFT, planar surface tensions $\gamma(\infty,\mu)$ at the respective chemical potentials; typically better than 1 part in 5×10^4. The fits also confirm that in the limit $R\to\infty$ and for $\delta\mu\neq0$ the leading-order correction to the planar surface tension is linear in the curvature; see Eq. (18). This contrasts with the situation when $\delta\mu=0$, i.e., $R_c=\infty$, where the surface tension has a nonanalytic $R^{-2/3}$ term (Fig. 6).

The difference between the surface tension at a spherical and at a planar substrate is plotted versus $(\beta\delta\mu)^{-1/3}$ for two different substrate radii in Figs. 9 and 10. The gradients of the linear fits are close to those predicted by Eq. (18). At

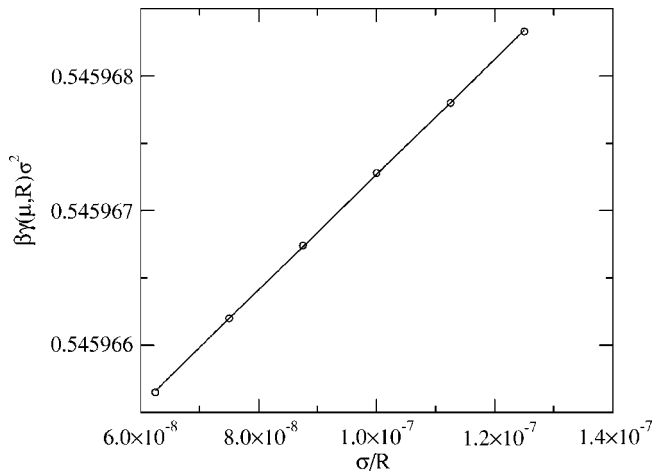

FIG. 7. The surface tension for liquids off coexistence, $\beta\delta\mu=4.78\times10^{-7}$ ($\sigma/R_c=2.85\times10^{-7}$), adsorbed at hard-spherical walls of radius $R-\sigma/2$, versus curvature for $T=0.7T_c$ (○). The straight line shows a linear fit to the DFT data [see Eq. (18)].

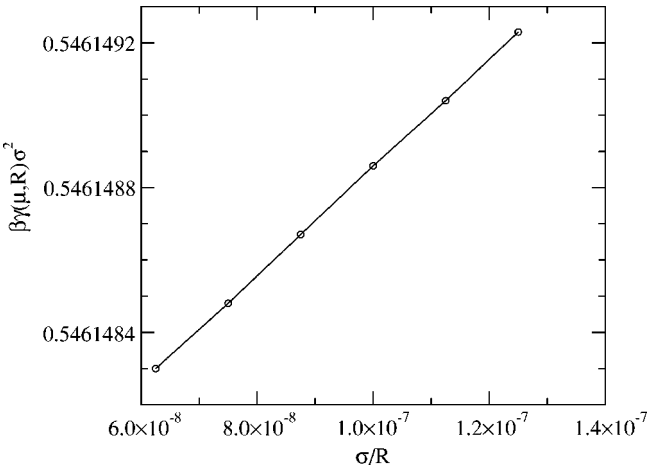

FIG. 8. As for Fig. 7 but with $\beta\delta\mu=1.53\times10^{-5}$ ($\sigma/R_c=9.11\times10^{-6}$).

larger values of $\delta\mu^{-1/3}$ the higher-order $R^{-2}\delta\mu^{-4/3}$ term becomes significant, causing the results to deviate from a straight line.

E. Contact density at the wall

In Fig. 11 we plot the difference between the contact densities at the wall for the coexisting liquid, $\rho_{liq}(R^+)\equiv\rho(R^+,\mu_{co}^{+})$, and gas, $\rho_{gas}(R^+)\equiv\rho(R^+,\mu_{co}^{-})$, phases versus curvature at $T=0.7T_c$. By subtracting the wall/gas contact density we eliminate the first two terms in Eq. (16) so that the leading-order term in the difference of contact densities is $2\beta\sigma^3\gamma_{gl}(\infty)/R$. By performing a least squares fit for $R/\sigma>10^6$ (see Fig. 11) we extract the gradient and compare with the independently calculated planar gas/liquid tension. The agreement is better than 1 part in 10^4. This confirms that the contact density at the wall/liquid interface $\rho(R^+,\mu_{co}^{+})$ does

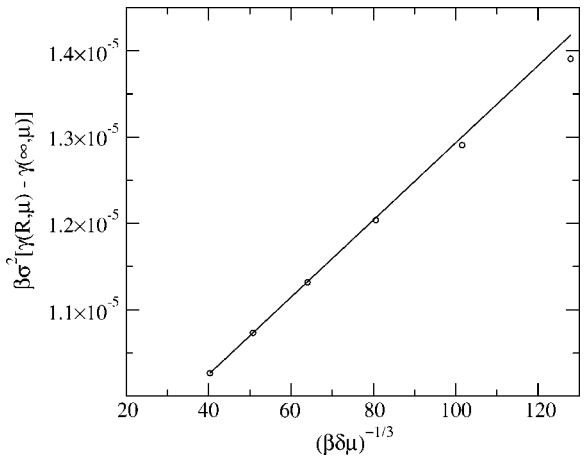

FIG. 9. The difference in surface tension between a spherical and a planar substrate versus $(\beta\delta\mu)^{-1/3}$, for the liquid adsorbed at a hard wall of radius $R-\sigma/2$ with $R=8\times10^6\sigma$, for $T=0.7T_c$ (○). The straight line shows a fit to the DFT data in the linear region and has gradient 4.47×10^{-8} (compared to a predicted gradient of 4.59×10^{-8}); see Eq. (18).

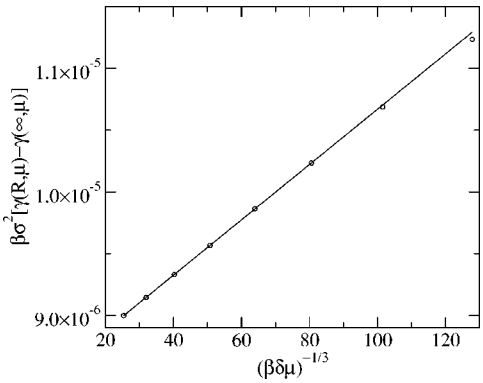

FIG. 10. As for Fig. 9 but with $R=1.6\times10^{7}\sigma$. The linear fit to the DFT data has gradient 2.24×10^{-8} (compared to a predicted gradient of 2.29×10^{-8}).

acquire a contribution proportional to the Laplace pressure of the gas/liquid interface located far from the wall, i.e., near $R+l_{eq}$, as $R^{-1}\to0$. A plot equivalent to Fig. 11 was presented in Fig. 2 of Ref. [9] for the case of a square-well fluid adsorbed at a hard-spherical wall. In the latter case there was good numerical evidence for the presence of the next to leading order $R^{-2}\ln(aR)$ term appropriate to short-range forces. However it was difficult to extract accurately the coefficient of this term. For the case of dispersion forces described here we are able to fit the difference in contact densities very accurately by including the $R^{-5/3}$ next to leading order term—see Eq. (16). The coefficient we obtain from the numerical fit agrees with the predicted value of $4\beta[\gamma_{gl}(\infty)^2b]^{1/3}$ to better than 0.5%.

Off coexistence the contact density at spherical substrates with large radii, chosen so that $R\gg R_c$, is expected to be linear in the curvature [Eq. (19)]. The predicted gradient is $2\beta\gamma_{wl}(\infty,\mu)$, where the planar wall/liquid surface tension at chemical potential μ can again be found independently. Figures 12 and 13 show graphs of contact density against curvature for two different, fixed chemical potentials. Once

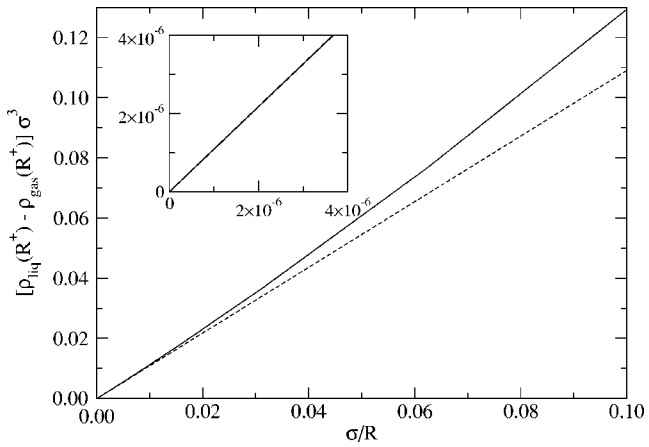

FIG. 11. The difference between contact densities in the liquid, $\mu_{co}^{+}(T)$, and gas, $\mu_{co}^{-}(T)$, phases adsorbed at hard-spherical walls of radii $R-\sigma/2$, versus curvature for $T=0.7T_c$ (full line). A fit to the linear portion near the origin (see inset for data at large R) is shown as a dotted line. The gradient is 1.0904, which is close to $2\beta\sigma^2\gamma_{gl}(\infty)=1.090\,39$ predicted by Eq. (16).

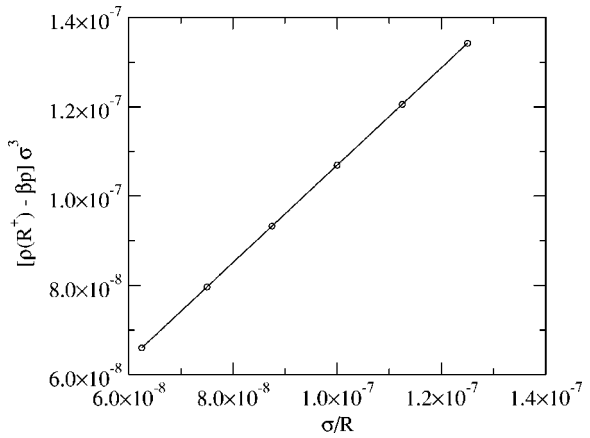

FIG. 12. The contact density for liquids off coexistence, $\beta\delta\mu=4.78\times10^{-7}$ ($\sigma/R_c=2.85\times10^{-7}$), adsorbed at hard spherical walls, as a function of the curvature. The gradient of the straight line fit is 1.09193 compared to a predicted gradient of 1.09191 -see Eq. (19). βp is the contact density at a planar wall, $R=\infty$, for a liquid at the same chemical potential deviation $\delta\mu$.

again the agreement between the gradients of the linear fits and those predicted by the theory is very good, to 1 part in 10^4. As emphasized in Ref. [6], it is important to confirm the validity of Eq. (19) since this is the route employed by Stillinger and Cotter [7] in their derivation of an exact formula for the planar hard-wall fluid surface tension. Note that for small values of $\beta\delta\mu$ very large radii R are required to enter the regime of validity of Eq. (19).

V. FLUID INSIDE A HARD SPHERICAL CAVITY

In this section we consider what happens when the curvature is negative, $R^{-1}<0$. The fluid is now adsorbed on the inside surface of the hard-spherical cavity as shown in Fig. 14. We can remain in the grand-canonical ensemble by allowing solvent particles to be "ghosted" into the sphere from a reservoir at fixed (μ,T). Once again we take $\delta\mu>0$ so that the reservoir is a liquid state. Following the coarse-grained Hamiltonian approach outlined in Sec. II we obtain the excess grand potential per unit area:

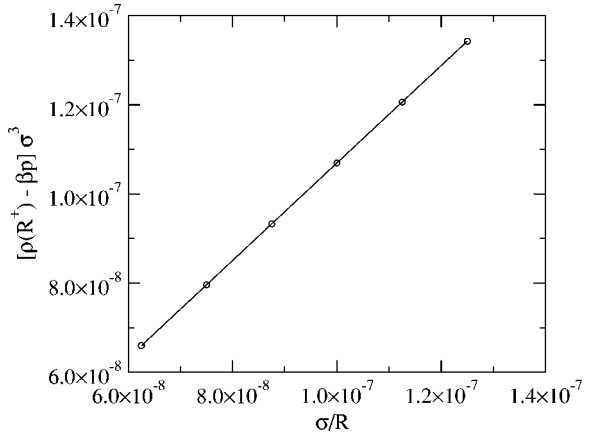

FIG. 13. As for Fig. 12 but with $\beta\delta\mu=1.53\times10^{-5}$ ($\sigma/R_c=9.11\times10^{-6}$). The gradient of the straight line fit is 1.092 33 compared to a predicted gradient of 1.092 28.

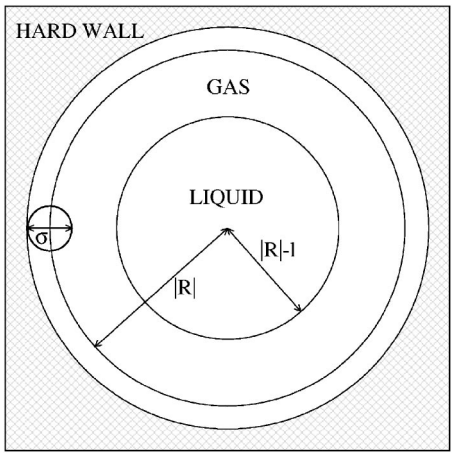

FIG. 14. The fluid inside a hard-spherical cavity, i.e., curvature $R^{-1}<0$, showing a fluid particle of diameter σ at the contact surface for the density profile. In the sharp-kink approximation there is a drying film with the gas density ρ_g^+ between $r=|R|$ and $r=|R|-l$, and the density in the central region $r<|R|-l$ is that of the bulk liquid ρ.

$$\frac{\Omega^{ex}}{A_{wg}} = \gamma_{wg}(R,\mu) + \gamma_{gl}(R)\left(1-\frac{2l}{|R|}\right) + \frac{b}{l^2} + (\rho_l-\rho_g)\delta\mu l \tag{30}$$

and minimizing with respect to l gives the equilibrium drying film thickness

$$l_{eq} = \left(\frac{2b}{(\rho_l-\rho_g)\delta\mu - 2\gamma_{gl}(\infty)/|R|}\right)^{1/3}. \tag{31}$$

The Laplace pressure from the curved liquid/gas interface now acts to *increase* the thickness of the gas layer and the equilibrium film thickness on the inside surface of the spherical hard wall is *greater* than that at the planar wall for the same value of $\delta\mu$; cf. Eq. (8).

For fixed, nonzero $\delta\mu$ the equilibrium film thickness is continuous through $R^{-1}=0$ and provided $|R|\gg R_c$ the wall/liquid surface tension has (apart from the ubiquitous $R^{-2}\ln|R|$ term) a power-series expansion in the curvature [see Eq. (18)]:

$$\gamma_{wl}(R,\mu) = \gamma_{wl}(\infty,\mu) + \frac{2\gamma_{gl}(\infty)}{R}\left(\frac{2b}{(\rho_l-\rho_g)\delta\mu}\right)^{1/3} + \frac{\Sigma\delta_T}{R} + O(R^{-2}\ln|R|) + O\left(\frac{R_c}{R}\right)^2. \tag{32}$$

As we decrease the size of the cavity further (i.e., the curvature R^{-1} becomes more negative) the film thickness l_{eq} increases and as we approach $R=-R_c$ the denominator in Eq. (31) vanishes, implying that the film thickness diverges. However, in finding the global minimum in the excess grand potential we must also consider the state in which the cavity is filled with the metastable gas phase, i.e., capillary evaporation [18] (see Fig. 15). The excess grand potential for this configuration is

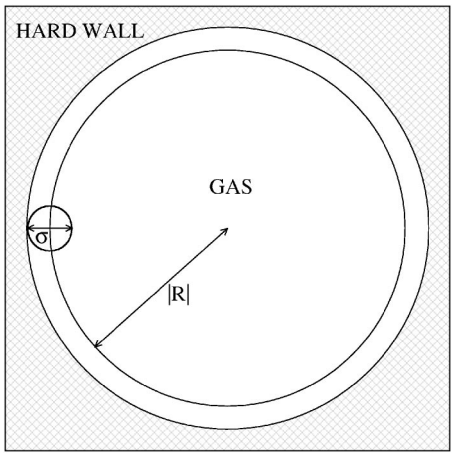

FIG. 15. Capillary evaporation in a hard-spherical cavity: In the sharp-kink approximation the cavity is filled with fluid with the gas density ρ_g^+.

$$\frac{\Omega_g^{ex}}{A_{wg}} \equiv \frac{\Omega + pV_{acc}}{A_{wg}} = \frac{1}{3}(\rho_l-\rho_g)\delta\mu|R|. \tag{33}$$

The equilibrium state is the state with the minimum excess grand potential per unit area. Therefore capillary evaporation occurs if $\Omega^{ex}=\Omega_g^{ex}$. Combining Eqs. (30), (31), and (33), we find that

$$(\rho_l-\rho_g)\delta\mu = \frac{3\gamma_{gl}(\infty)}{(R_{evap}-3l_{eq}/2)} \tag{34}$$

or

$$R_{evap} - \frac{3l_{eq}}{2} = \frac{3R_c}{2} \tag{35}$$

for R_{evap}, the radius $|R|$, for which capillary evaporation occurs at fixed $\delta\mu$. l_{eq} is given by Eq. (31). [The equivalent result for a system with short-ranged interparticle forces is $(\rho_l-\rho_g)\delta\mu=3\gamma_{gl}(\infty)/(R_{evap}-l_{eq})$, where we have assumed $l_{eq}\gg$ bulk correlation length of the gas phase.] Thus evaporation occurs before we reach the nonanalytic regime $R=-R_c$, i.e., $R_{evap}>R_c$. As we decrease the radius of the cavity through $|R|=R_{evap}$ there is a discontinuous (first-order) phase transition from a state in which the cavity contains liquid with a finite film of gas next to the surface to a state where the hard-spherical cavity is completely filled with the gas phase. However, on decreasing $\delta\mu$, R_c increases so that the validity of Eq. (32) is restricted to large values of $|R|$ and R_{evap} is larger. In the limit $\delta\mu\to 0^+$, bulk coexistence, there is complete drying at the planar wall and introducing *infinitesimal* negative curvature results in the hard cavity being filled with the gas phase, i.e., capillary evaporation occurs immediately.

We should emphasize that the treatment of evaporation presented above is mean field in character. For a finite interior radius $|R|$ there is, of course, no true phase transition as a finite volume of fluid is involved. Nevertheless, for a large radius $\gg\sigma$ we expect the first-order evaporation transition to be only weakly rounded, in say $\delta\mu$, so that the adsorption Γ (order parameter) would not exhibit a discontinuous jump;

rather, it would show an extremely rapid change in slope. Such a consideration does not affect the overall validity of the arguments regarding crossover from nonanalytic to analytic behavior and the onset of evaporation.

VI. CONCLUSIONS

In this paper we have investigated the effects of curvature on the adsorption properties of a simple fluid, described by the fluid-fluid pair potential of Eq. (21), near a hard-spherical wall. We find that the results of a microscopic DFT approach (see Sec. IV) are completely consistent with those predicted by a coarse-grained effective interfacial Hamiltonian in Sec. II. The main conclusions are as follows.

(1) We confirm (see Fig. 3) the sharp-kink prediction that there is an $R^{-2}\ln R$ term in the surface tension of a fluid with an attractive $-r^{-6}$ tail in the pair potential by considering the gas at $\mu=\mu_{co}^{-}$ adsorbed at a hard-spherical wall. However, the leading-order correction to the planar surface tension is proportional to R^{-1}.

(2) Our DFT results for the Gibbs adsorption Γ (see Fig. 5) confirm that the thickness of the drying film diverges as $R^{1/3}$, as $R\to\infty$, for our model fluid at bulk coexistence $\delta\mu=0^{+}$, in agreement with earlier predictions [12–14]. Moreover, the excellent data collapse in DFT results for Γ demonstrates that the isomorphism between the undersaturation pressure $(\rho_l-\rho_g)\delta\mu$ at a planar substrate and the Laplace pressure $2\gamma_{gl}(\infty)/R$ remains valid down to rather small radii R, where thick drying films are no longer present. This suggests that as regards the adsorption (and therefore the binding potential) the isomorphism may be valid beyond leading order. Note that the total surface tension for these two systems is not expected to be the same beyond leading order because of the R^{-1} terms in the individual wall/gas and gas/liquid surface tensions which arise if the density profile is not sharp-kink-like.

(3) We have shown (see Fig. 6) that the wall/liquid surface tension for $\delta\mu=0^{+}$ has a leading-order $R^{-2/3}$ correction to the planar result. In addition we have confirmed that the coefficient of this contribution [see Eq. (14)] calculated from DFT is the same as that predicted by the coarse-grained Hamiltonian, with the parameter b given by the sharp-kink approximation, i.e., Eq. (6).

(4) DFT results (see Fig. 11) confirm the validity of the predictions of Eq. (16) for the contact density $\rho(R^{+},\mu)$ at $\delta\mu=0^{+}$, namely, $k_BT\rho(R^{+},\mu_{co}^{+})$ has a contribution proportional to the Laplace pressure $2\gamma_{gl}(\infty)/R$ plus a term in $R^{-5/3}$. The DFT results for the coefficients of both the R^{-1} and $R^{-5/3}$ terms are in excellent agreement with those predicted by the effective interfacial Hamiltonian.

(5) In the analytic regime $R>R_c$, which requires $\delta\mu>0$, the theory of Sec. II predicts that the surface tension and the contact density should possess a power series expansion in the curvature R^{-1}. Our DFT results (see Figs. 7–10, 12, and 13) confirm this prediction. In particular, the coefficient of R^{-1} in the expansion of $k_BT\rho(R^{+},\mu)$ yields the planar surface tension $\gamma_{wl}(\infty,\mu)$—see Eq. (19)—as is required in the classic analysis of Ref. [7].

(6) We find that the isomorphism between a system at a planar substrate off coexistence by an amount $\delta\mu$ and one at a spherical substrate at $\delta\mu=0^{+}$ whose radius is given by $2\gamma_{gl}(\infty)/R=(\rho_l-\rho_g)\delta\mu$ applies to the *whole* density profile, provided the hard cavity radius $R\geqslant 100\sigma$. There is no obvious reason why this isomorphism should remain valid down to such small radii. We know that in the limit of large R the drying film thickness and therefore the adsorption Γ should be equivalent. We also know that the contact densities should be equivalent since these can be viewed as thermodynamic quantities determined by the surface tension—see Eq. (15). But there is no compelling reason to expect that the profiles themselves would be very close for such a wide range of R.

Our DFT results refer to a single temperature $T=0.7T_c$. We have carried out a few calculations for another temperature $T=0.6T_c$. The results are in equally good agreement with the predictions of Sec. II.

Both theoretical approaches employed here omit effects of capillary-wave fluctuations in the gas-liquid interface that develop near $r=R+l_{eq}$. For complete wetting/drying at a planar interface when dispersion forces (power-law interaction potentials) are present, fluctuations are not expected to alter the results of the corresponding mean-field treatment [29]. This follows since the upper critical dimension d_c for the complete wetting phase transition is $d_c=(2+3n)/(2+n)$ where n is the exponent describing the decay of the binding potential $w(l;\infty)\sim l^{-n}$; recall that $n=2$ for dispersion forces in $d=3$ [see Eq. (5)]. Thus for any finite n, $d_c<3$ [10,11,29], and fluctuations should not affect the results of a mean-field analysis of complete drying at a planar surface. Since, to leading order in l/R, incorporating curvature simply replaces $(\rho_l-\rho_g)\delta\mu$ at a planar wall by the sum $(\rho_l-\rho_g)\delta\mu+2\gamma_{gl}(\infty)/R$ we conjecture that our mean-field results for nonanalytic contributions to interfacial properties should be unaltered by incorporating capillary wave fluctuations, i.e., our predicted power laws and amplitudes should be *exact* [30].

Of course the same conclusion holds for a model fluid with $n\neq 2$, i.e., one for which the fluid-fluid pair potential decays as $-r^{-(n+4)}$. Often it is useful to consider these more general models in the statistical mechanics of wetting [29]. For such a model $l_{eq}\sim R^{1/(n+1)}$ for $\delta\mu=0^{+}$, $\gamma_{wl}(R,\mu_{co}^{+})$ acquires a term in $R^{-n/(n+1)}$, and $\rho(R^{+},\mu_{co}^{+})$ a term in $R^{-(2n+1)/(n+1)}$.

When comparing our results with those derived for short-ranged potentials [6,9] there are two key differences: (i) drying in a fluid where dispersion forces are present leads to stronger (power-law) nonanalytic contributions than the logarithmic contributions which characterize drying with short-ranged forces and (ii) the $-r^{-6}$ decay of the interparticle potential results in wall/gas and gas/liquid interfacial tensions that include a term in $R^{-2}\ln R$ associated with the density difference between the relevant bulk phases. Note that we have not attempted to confirm the predicted $R^{-2}\ln R$ term in the gas/liquid tension using DFT.

We conclude by turning to the physical relevance of our results. There are several applications in fluid interfacial phenomena where it would be advantageous to be able to express the interfacial free energy as an expansion in powers of

the relevant curvature(s). A well-known example is Helfrich's analysis of fluctuating membranes [31]. Recently König *et al.* [8] have provided arguments as to why it should be possible to expand the wall/fluid surface tension $\gamma_{wf}(R,\mu)$ and other surface thermodynamic quantities as a constant plus a contribution linear in the mean curvature and one linear in the Gaussian curvature of the convex surface bounding the fluid. If one can make such an expansion this would be most useful in colloid science for theories of depletion forces for hard particles of various shapes [5,8]. Our present work, as well as that in Ref. [6], shows that for a fluid undergoing gas-liquid coexistence it is not, *in general*, possible to make such power-series expansions. These must fail near the bulk critical point where the correlation length becomes comparable with the radius R and here we have demonstrated that the series expansion breaks down, because of drying, in the regime $\sigma \ll R < R_c$. For the regime $R > R_c$ a power-series expansion in the curvature(s) should exist for short-ranged fluid-fluid potentials [6] but, as we have seen here, dispersion forces give rise to additional $R^{-2}\ln R$ contributions to the surface tensions—see also Ref. [12]. Clearly the value of R_c is important. As emphasized earlier, R_c for water at room temperature and pressure is surprisingly large—about 1 μm. This follows because $\beta\delta\mu$, or equivalently $\beta\sigma^3[p-p_{co}(T)]$, is so small. The same remark should hold for many other liquids at atmospheric pressure. The implication is that for many liquids one is usually in the nonanalytic regime $R < R_c$, where the power-series expansions are not applicable.

This observation has repercussions for the solvation of big solvophobic solute particles. Recall from the definition in Eq. (2) that the work required to create an empty cavity of radius R (equivalent to the excess chemical potential for inserting a single hard sphere) in the fluid at fixed (μ,T) is

$$\mu_{hs}^{ex}(R,\mu) = p\tfrac{4}{3}\pi R^3 + 4\pi R^2 \gamma_{wf}(R,\mu) \tag{36}$$

where $p(\mu,T)$ is the pressure of the reservoir. For a liquid such as water under ambient conditions, where $\beta\sigma^3 p$ is very small, the second, interfacial, term in Eq. (36) plays a very important role and several authors [23,32] have emphasized that $\gamma_{wl}(R,\mu)$ will, because of drying, contain a (large) gas-liquid surface tension contribution for large solute radii. Here we have shown that the work of cavity insertion per unit area contains a positive nonanalytic leading-order correction term proportional to $R^{-2/3}$ in addition to the term $\gamma_{gl}(\infty)$—see Eq. (14), provided $R < R_c$. We shall discuss the implications of this result for the solvation of a hard sphere in a later publication.

In real systems it is very difficult to create situations where the wall-fluid potential is perfectly hard, although refractive index matching might bring about a good approximation in colloidal fluids. In practice there are often (weak) residual attractive interactions between the big particle and the fluid. Provided the wall-fluid interparticle potential decays no more slowly than r^{-6} and complete drying still occurs $\gamma_{wl}(R,\mu_{co}^{+})$ will acquire a $R^{-2/3}$ contribution. However, if these residual interactions are sufficiently attractive then one does not have complete drying. Rather one has solvophobic (hydrophobic) substrates that correspond in the planar limit to partial drying, i.e., the contact angle $\theta < 180°$ rather than $\theta = 180°$, corresponding to complete drying. In this case a thick (diverging) drying film of gas does not develop at the planar wall/liquid interface but there can still be a region of depleted fluid density with an accompanying (large) wall/liquid surface tension. Solvation under such circumstances is, of course, of much relevance in physical chemistry as is the transition from complete to partial drying. If the latter is continuous (critical drying) new nonanalytic contributions arise near the transition for the surface tension and for other interfacial quantities; when dispersion forces are present these are power-law contributions, different from those associated with complete wetting [33].

As remarked in Sec. I and in Ref. [6] our theory is also relevant to the case of wetting of a curved substrate by a liquid film, $\mu \to \mu_{co}^{-}(T)$, or of a colloidal particle near phase separation in a binary solvent. In both cases we expect to find equivalent regimes of interfacial behavior, defined by length scales equivalent to R_c.

ACKNOWLEDGMENTS

We have benefited from conversations with A. J. Archer, S. Dietrich, P. Bryk, J. R. Henderson, M. Oettel, and J. Stecki. R. Roth provided much valuable advice and guidance in the early stages of our numerical calculations. We are grateful for his assistance, for sharing his ideas, both experimental and theoretical, on capillary evaporation during discussions at the Institute "Zum Paulaner" and for valuable comments on the manuscript. M.C.S. was supported by EPSRC.

APPENDIX: THE SHARP-KINK APPROXIMATION FOR THE SURFACE TENSION AND BINDING POTENTIAL

The sharp-kink approximation assumes that the fluid density is constant on each side of the interface, with a discontinuous jump at the interface. The surface tension is calculated by comparing the free energy of the system with that of a semi-infinite amount of each of the two uniform fluid phases [10]. A wall/fluid interface is treated in a very similar way to a fluid/fluid interface. For a hard wall which does not exert any attractive force on the fluid particles the wall density ρ_w is simply set to zero in the following equations.

Planar interface

In order to construct the interface imagine breaking an infinite amount of uniform fluid, number density ρ_1, in half. The potential due to a semi-infinite slab of fluid distance z' away is

$$\rho_1 v(z') = \rho_1 \int_{z'}^{\infty} dz \int_0^{\infty} 2\pi r \phi_{att}(\sqrt{r^2+z^2}) dr \tag{A1}$$

where $\phi_{att}(r_{12})$ is the attractive interaction potential between fluid particles separated by distance r_{12}. Carrying out the integration for the attractive part of a Lennard-Jones potential, defined by Eq. (21), gives

$$v(z') = \begin{cases} 4\pi\epsilon\left(\dfrac{\sigma^{12}}{45z'^9} - \dfrac{\sigma^6}{6z'^3}\right), & z' > r_{min}, \\ 4\pi\epsilon\left[\dfrac{r_{min}^2 z'}{4} - \dfrac{z'^3}{12} - \dfrac{r_{min}^3}{6} + \dfrac{2\sigma^{12}}{9r_{min}^9} - \dfrac{2\sigma^6}{3r_{min}^3} - \left(\dfrac{\sigma^{12}}{5r_{min}^{10}} - \dfrac{\sigma^6}{2r_{min}^4}\right)z'\right], & z' < r_{min}. \end{cases} \tag{A2}$$

The free-energy cost (per unit area of interface) for breaking apart the fluid is

$$-\frac{\rho_1^2}{2}\int_0^\infty v(z')dz' \tag{A3}$$

and similarly for the second fluid of density ρ_2,

$$-\frac{\rho_2^2}{2}\int_0^\infty v(z')dz'. \tag{A4}$$

Bringing the two semi-infinite pieces together increases the free energy by

$$+\rho_1\rho_2\int_0^\infty v(z')dz' \tag{A5}$$

per unit area. The surface tension for the planar fluid/fluid interface is therefore

$$\gamma_{12}(\infty) = -\frac{(\Delta\rho)^2}{2}\int_0^\infty v(z')dz' \tag{A6}$$

where $\Delta\rho \equiv \rho_1 - \rho_2$. Thus for a liquid/gas interface, $\Delta\rho = \rho_l - \rho_g$, the difference in coexisting densities. For the potential in Eq. (A2), $\gamma_{12}(\infty)$ is calculated to be

$$\gamma_{12}(\infty) = \frac{9}{16}(\Delta\rho)^2\pi\epsilon r_{min}^4. \tag{A7}$$

The analogous expression for the surface tension between a solid wall of density ρ_w and a fluid of density ρ_1 is

$$\gamma_{wf}(\infty) = \tfrac{9}{16}\pi(\rho_1^2\epsilon r_{min}^4 - 2\rho_1\rho_w\epsilon_{wf}r_{min,wf}^4), \tag{A8}$$

where ϵ_{wf} and $r_{min,wf}$ refer to the interaction potential between wall and fluid particles, taken to be the same form as Eq. (21).

Spherical interface

The potential at a distance r' from the center of the sphere of fluid, number density ρ_1, radius R ($R < r'$), is

$$\begin{aligned}\rho_1 v(r',R) &= \rho_1\int_{r\le R} d\mathbf{r}\ \phi_{att}(|\mathbf{r}' - \mathbf{r}|) \\ &= \rho_1\int_{-R}^{R} dz\int_0^{\sqrt{R^2-z^2}} 2\pi s\,\phi_{att}\left[\sqrt{(r'-z)^2 + s^2}\right]ds\end{aligned}$$

where $s^2 = x^2 + y^2$ and $v(r',R)$ is rotationally invariant so we have taken $\mathbf{r}'$ to lie along the z axis for the purpose of evaluating the integral. For the Lennard-Jones attractive potential of Eq. (21) integration gives

$$v(r',R) = \begin{cases} 4\pi\epsilon\Bigg(-\dfrac{4r_{min}^3}{9} - \dfrac{R^3}{6} - \dfrac{r'^3}{48} + \dfrac{9r_{min}^2 r'}{40} + \dfrac{R^2 r'}{8} + \dfrac{9r_{min}^4}{32r'} \\ \quad - \dfrac{9R^2 r_{min}^2}{40r'} + \dfrac{R^4}{16r'} + \dfrac{\sigma^{12}}{40r'(r'+R)^8} - \dfrac{\sigma^6}{4r'(r'+R)^2} - \dfrac{\sigma^{12}}{45(r'+R)^9} + \dfrac{\sigma^6}{6(r'+R)^3}\Bigg), & R < r' < R + r_{min}, \\ 4\pi\epsilon\Bigg(-\dfrac{\sigma^{12}}{40r'(r'-R)^8} + \dfrac{\sigma^6}{4r'(r'-R)^2} + \dfrac{\sigma^{12}}{45(r'-R)^9} - \dfrac{\sigma^6}{6(r'-R)^3} \\ \quad + \dfrac{\sigma^{12}}{40r'(r'+R)^8} - \dfrac{\sigma^6}{4r'(r'+R)^2} - \dfrac{\sigma^{12}}{45(r'+R)^9} + \dfrac{\sigma^6}{6(r'+R)^3}\Bigg), & r' > R + r_{min}. \end{cases} \tag{A9}$$

The surface tension for a spherical fluid/fluid interface of radius R is

$$\gamma_{12}(R) = -\frac{(\Delta\rho)^2}{2}\int_R^\infty \frac{r'^2}{R^2}v(r',R)dr'. \tag{A10}$$

Using Eq. (A9) one obtains the sharp-kink approximation for the surface tension:

$$\gamma_{12}(R) = (\Delta\rho)^2 \pi \epsilon r_{min}^4 \left(\frac{9}{16} - \frac{1}{12}\frac{\ln(2R/r_{min})}{(R/r_{min})^2} - \frac{5}{72}\frac{1}{(R/r_{min})^2} - \frac{1}{110\,592}\frac{1}{(R/r_{min})^8} \right) \tag{A11}$$

$$= \gamma_{12}(\infty)\left(1 - \frac{4}{27}\frac{\ln(2R/r_{min})}{(R/r_{min})^2} - \frac{10}{81}\frac{1}{(R/r_{min})^2} - \frac{1}{62\,208}\frac{1}{(R/r_{min})^8} \right) \tag{A12}$$

for $R > r_{min}$ (cf. [12,20]). The same formula is valid for the tension between a spherical solid wall and a fluid of density ρ_1 provided $\gamma_{12}(\infty)$ is replaced by $\gamma_{wf}(\infty)$, Eq. (A8).

The interaction between the interfaces

If the thickness l of the drying film is not infinite (see Figs. 1 and 2) then there will be an additional term in the grand potential due to the interaction between the wall/gas and the gas/liquid interfaces. For long-ranged interparticle forces the dominant contribution is from the tails of the fluid-fluid potentials, which decay as inverse powers of distance. In the sharp-kink approximation the extra free energy per unit area for the planar interface is

$$\omega(l;\infty) = -\rho_g(\rho_l - \rho_g)\int_l^\infty v(z')dz' \tag{A13}$$

where the wall density ρ_w has been set to zero for simplicity. Integration gives the binding potential of Eq. (5). The equivalent expression for a spherical interface is

$$\omega(l;R) = -\rho_g(\rho_l - \rho_g)\int_{l+R}^\infty \frac{r'^2}{R^2} v(r',R)dr' = \omega(l;\infty)\left[1 + \frac{l}{R} + O\left(\frac{l^2}{R^2}\ln(l/2R) \right) \right]. \tag{A14}$$

The leading-order correction to the planar result is consistent with the scaling form given by Eqs. (2.39) and (2.40) of Ref. [12].

[1] J. W. Gibbs, *The Collected Works of J. Willard Gibbs* (Longmans, Green, London, 1928), Vol. 1.
[2] J. R. Henderson, in *Fluid Interfacial Phenomena*, edited by C. A. Croxton (Wiley, New York, 1986), p. 555.
[3] J. R. Henderson, in *Fundamentals of Inhomogeneous Fluids*, edited by D. Henderson (Dekker, New York, 1992), p. 23.
[4] See, e.g., S. Dietrich, in *New Approaches to Problems in Liquid State Theory*, edited by C. Caccamo *et al.* (Kluwer, Dordrecht, 1999), p. 197.
[5] P. Bryk, R. Roth, K. R. Mecke, and S. Dietrich, Phys. Rev. E **68**, 031602 (2003), and references therein.
[6] R. Evans, J. R. Henderson, and R. Roth, J. Chem. Phys. **121**, 12074 (2004).
[7] F. H. Stillinger and M. A. Cotter, J. Chem. Phys. **55**, 3449 (1971).
[8] P. König, R. Roth, and K. R. Mecke, Phys. Rev. Lett. **93**, 160601 (2004).
[9] R. Evans, R. Roth, and P. Bryk, Europhys. Lett. **62**, 815 (2003).
[10] S. Dietrich, in *Phase Transitions and Critical Phenomena*, edited by C. Domb and J. Lebowitz (Academic Press, London, 1988), Vol. 12, p. 1.
[11] M. Schick, in *Liquids at Interfaces*, Les Houches Summer School Lectures, Session XLVIII, 1988 Proceedings of the Les Houches Summer School Lectures, Session XLVIII, edited by J. Charvolin, J. F. Joanny, and J. Zinn-Justin (Elsevier, Amsterdam, 1990), p. 416.
[12] T. Bieker and S. Dietrich, Physica A **252**, 85 (1998), and references therein.
[13] F. Brochard, J. Chem. Phys. **84**, 4664 (1986).
[14] T. Gil and L. V. Mikheev, Phys. Rev. E **52**, 772 (1995).
[15] R. Holyst and A. Poniewierski, Phys. Rev. B **36**, 5628 (1987).
[16] M. P. Gelfand and R. Lipowsky, Phys. Rev. B **36**, 8725 (1987).
[17] P. J. Upton, J. O. Indekeu, and J. M. Yeomans, Phys. Rev. B **40**, 666 (1989).
[18] R. Evans, J. Phys.: Condens. Matter **2**, 8989 (1990).
[19] Y. Rosenfeld, Phys. Rev. Lett. **63**, 980 (1989).
[20] M. A. Hooper and S. Nordholm, J. Chem. Phys. **81**, 2432 (1984); see also E. M. Blokhuis and D. Bedeaux, Physica A **184**, 42 (1992).
[21] C. Bauer, T. Bieker, and S. Dietrich, Phys. Rev. E **62**, 5324 (2000), and references therein.
[22] A. J. Archer, R. Evans, and R. Roth, Europhys. Lett. **59**, 526 (2002); A. J. Archer and R. Evans, J. Chem. Phys. **118**, 9726 (2003).
[23] See, e.g., K. Lum, D. Chandler, and J. D. Weeks, J. Phys. Chem. B **103**, 4570 (1999).
[24] R. C. Tolman, J. Chem. Phys. **17**, 333 (1949).
[25] A. Poniewierski and J. Stecki, J. Chem. Phys. **106**, 3358 (1997).
[26] M. P. Moody and P. Attard, J. Chem. Phys. **115**, 8967 (2001).
[27] A. E. van Giessen and E. M. Blokhuis, J. Chem. Phys. **116**, 302 (2002).
[28] R. Evans, in *Fundamentals of Inhomogeneous Fluids*, edited by D. Henderson (Dekker, New York, 1992), p. 85.
[29] R. Lipowsky, Phys. Rev. Lett. **52**, 1429 (1984).
[30] Of course, in an exact treatment one should employ the exact coexisting densities and planar surface tension in the relevant formulas.
[31] W. Helfrich, Z. Naturforsch. C **28**, 693 (1973).
[32] J. R. Henderson, J. Chem. Phys. **116**, 5039 (2002).
[33] M. C. Stewart (unpublished).